Measuring sparingly-soluble, aqueous salt crystallization kinetics using CSTRs-in-series: methodology development and $CaCO_3$ studies

Science and Technology Program
Research and Development Office
Final Report No. ST-2020-7120

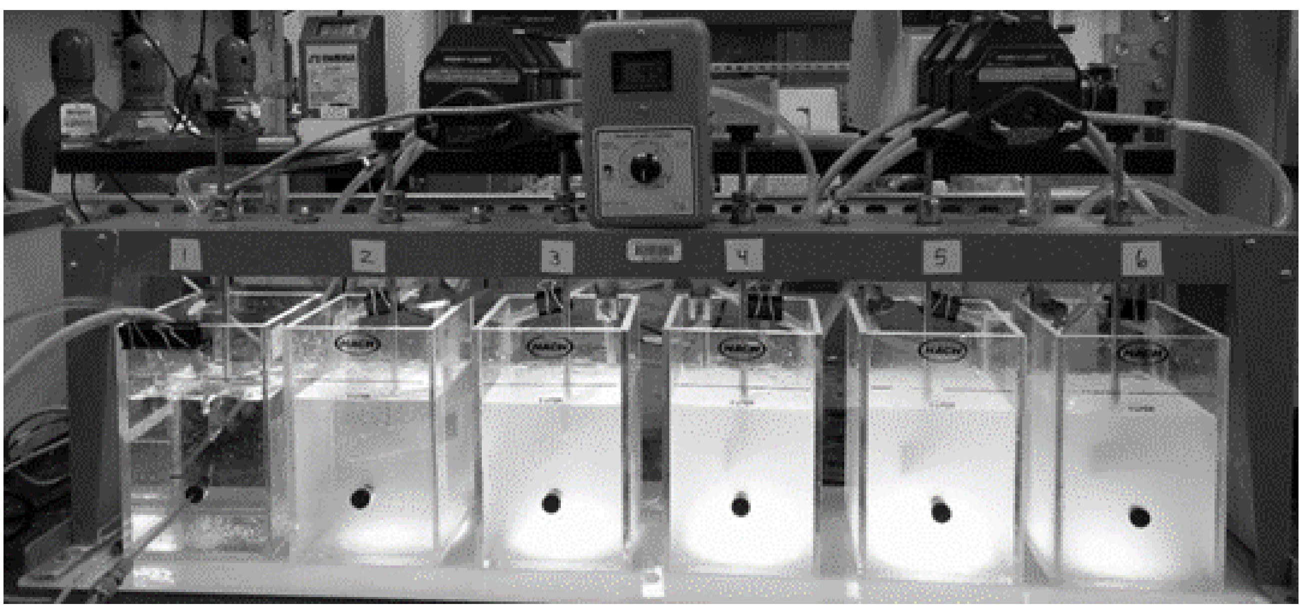

U.S. Department of the Interior

September 17, 2020

REPORT DOCUMENTATION PAGE	*Form Approved* *OMB No. 0704-0188*

1. REPORT DATE ***(DD-MM-YYYY)***	**2. REPORT TYPE**	**3. DATES COVERED** *(From - To)*
09/17/2020	Research	2018 - 2020

4. TITLE AND SUBTITLE
Measuring sparingly-soluble, aqueous salt crystallization kinetics using CSTRs-in-series: methodology development and CaCO3 studies

5a. CONTRACT NUMBER
19XR0680A1-RY154120601000202/CRYK1

5b. GRANT NUMBER
NA

5c. PROGRAM ELEMENT NUMBER
1541 (S&T)

6. AUTHOR(S)
Sankaranarayanan A. Ravichandran[1], Jordan Krist[2], Dakota Edwards[1], Saied Delagah[3], John Pellegrino[1]

5d. PROJECT NUMBER
Final Report ST-2020-Project ID-7120

5e. TASK NUMBER
NA

5f. WORK UNIT NUMBER
NA

7. PERFORMING ORGANIZATION NAME(S) AND ADDRESS(ES)
[1]Department of Mechanical Engineering, University of Colorado, Boulder, CO USA
[2]Department of Chemical and Biological Engineering, University of Colorado, Boulder, CO USA
[3]Bureau of Reclamation, Denver, CO USA

8. PERFORMING ORGANIZATION REPORT NUMBER

9. SPONSORING/MONITORING AGENCY NAME(S) AND ADDRESS(ES)
Science and Technology Program
Research and Development Office
Bureau of Reclamation
U.S. Department of the Interior
Denver Federal Center
PO Box 25007, Denver, CO 80225-0007

10. SPONSOR/MONITOR'S ACRONYM(S)
Reclamation

11. SPONSOR/MONITOR'S REPORT NUMBER(S)
Final Report ST-2020-Project ID-7120

12. DISTRIBUTION/AVAILABILITY STATEMENT
Final Report may be downloaded from https://www.usbr.gov/research/projects/index.html

13. SUPPLEMENTARY NOTES

14. ABSTRACT
We present a methodology and results for measuring crystallization kinetics of sparingly-soluble salt mixtures typical of reject/concentrate streams from membrane-based, inland water supply processes. More usable water can be recovered (and lower disposal costs incurred) from these concentrate streams through efficient crystallization. In this work, we present a steady state, continuous stirred tank reactors (CSTRs)-in-series approach to study crystallization kinetics of a model solution mixture that is supersaturated in $CaCO_3$. We have used pH, conductivity and turbidity changes in the system to monitor crystallization. We examined how mixing energy dissipation affects the induction times for crystallization. Notably, discernible crystallization could only be advanced to the 1st CSTR by using a recirculation loop to "fine-tune" the effect of surface area exposure-to-volume ratio, as well as, mixing energy dissipation. A rudimentary, semi-empirical model was used to capture the parametric trends of our experimental results, using the Kolmogorov mixing lengths, surface area-to-volume ratios, flow rates, and nominal diffusion coefficients. This parameterization may be tested further for design scale-up guidance.

15. SUBJECT TERMS
Crystallization Kinetics, Desalination Concentrate,

16. SECURITY CLASSIFICATION OF:			**17. LIMITATION OF ABSTRACT**	**18. NUMBER OF PAGES**	**19a. NAME OF RESPONSIBLE PERSON**
					Saied Delagah
a. REPORT	**b. ABSTRACT**	**THIS PAGE**			**19b. TELEPHONE NUMBER** *(Include area code)*
U	U	U			303-912-6793

Mission Statements

The Department of the Interior (DOI) conserves and manages the Nation's natural resources and cultural heritage for the benefit and enjoyment of the American people, provides scientific and other information about natural resources and natural hazards to address societal challenges and create opportunities for the American people, and honors the Nation's trust responsibilities or special commitments to American Indians, Alaska Natives, and affiliated island communities to help them prosper.

The mission of the Bureau of Reclamation is to manage, develop, and protect water and related resources in an environmentally and economically sound manner in the interest of the American public.

Disclaimer

Information in this report may not be used for advertising or promotional purposes. The data and findings should not be construed as an endorsement of any product or firm by the Bureau of Reclamation, Department of Interior, or Federal Government. The products evaluated in the report were evaluated for purposes specific to the Bureau of Reclamation mission. Reclamation gives no warranties or guarantees, expressed or implied, for the products evaluated in this report, including merchantability or fitness for a particular purpose.

Acknowledgements

The Science and Technology Program, Bureau of Reclamation, sponsored this research. This research study was published in a peer review journal and the primary author of the paper, Sankaranarayanan A. Ravichandrana, should be recognized.

Measuring sparingly-soluble, aqueous salt crystallization kinetics using CSTRs-in-series: methodology development and CaCO3 studies

Final Report No. ST-2020-7120

prepared by *Saied Delagah, Civil Engineer, Technical Services Center*

Peer Review

Bureau of Reclamation
Research and Development Office
Science and Technology Program

Final Report No. ST-2020-7120

Measuring sparingly-soluble, aqueous salt crystallization kinetics using CSTRs-in-series: methodology development and CaCO3 studies

SAIED DELAGAH
Digitally signed by SAIED DELAGAH
Date: 2020.10.02 09:28:26 -06'00'

Prepared by: Saied Delagah
Civil Engineer, Bureau of Reclamation, Technical Services Center

ROBERT JURENKA
Digitally signed by ROBERT JURENKA
Date: 2020.10.02 09:17:13 -06'00'

Peer Review by: Robert Jurenka
Civil Engineer, Bureau of Reclamation, Technical Services Center

Contents

Executive Summary

We present a methodology and results for measuring crystallization kinetics of sparingly-soluble salt mixtures typical of reject/concentrate streams from membrane-based, inland water supply processes. More usable water can be recovered (and lower disposal costs incurred) from these concentrate streams through efficient crystallization. In this work, we present a steady state, continuous stirred tank reactors (CSTRs)-in-series approach to study crystallization kinetics of a model solution mixture that is supersaturated in CaCO3. We have used pH, conductivity and turbidity changes in the system to monitor crystallization using six CSTRs with individual residence times of nominally 3, 5, and 11 min. This system operates in a steady state mode with total crystallization times from ~ 15-68 min and was capable of handling up to ~0.59 L/min of hard water for the shortest residence time studied. The supersaturation was depleted ~25% and over 50% with total reactor system residence times of ~15 and 68 min, respectively, without any added chemicals. Using the metric of 5 NTU turbidity as being the point of discernible crystal formation, we examined how mixing energy dissipation affects the induction times for crystallization. Notably, discernible crystallization could only be advanced to the 1st CSTR by using a recirculation loop to "fine-tune" the effect of surface area exposure-to-volume ratio as well as mixing energy dissipation. A rudimentary, semi-empirical model was used to capture the parametric trends of our experimental results, using the Kolmogorov mixing lengths, surface area-to-volume ratios, flow rates, and nominal diffusion coefficients. This parameterization may be tested further for design scale-up guidance.

This paper was published in the following peer reviewed journal:
Sankaranarayanan A. Ravichandran, Jordan Krist, Dakota Edwards, Saied Delagah, John Pellegrino, Measuring sparingly-soluble, aqueous salt crystallization kinetics using CSTRs-in-series: Methodology development and $CaCO_3$ studies, Separation and Purification Technology, Volume 211, 2019, Pages 408-420, ISSN 1383-5866, https://doi.org/10.1016/j.seppur.2018.09.084.

Appendix A contain this peer reviewed article in lieu of the body in this report.

Reference to Peer Reviewed Journal Article

Please see Appendix A for the peer reviewed publication that will serve as the final report for this project and associated citation:

Sankaranarayanan A. Ravichandran, Jordan Krist, Dakota Edwards, Saied Delagah, John Pellegrino, Measuring sparingly-soluble, aqueous salt crystallization kinetics using CSTRs-in-series: Methodology development and $CaCO_3$ studies, Separation and Purification Technology, Volume 211, 2019, Pages 408-420, ISSN 1383-5866, https://doi.org/10.1016/j.seppur.2018.09.084.

Appendix A

Measuring sparingly-soluble, aqueous salt crystallization kinetics using CSTRs-in-series: methodology development and $CaCO_3$ studies

Sankaranarayanan A. Ravichandran[a], Jordan Krist[b], Dakota Edwards[a], Saied Delagah[c], John Pellegrino[a,*]
[1]Department of Mechanical Engineering, University of Colorado, Boulder, CO USA
[2]Department of Chemical and Biological Engineering, University of Colorado, Boulder, CO USA
[3]Bureau of Reclamation, Denver, CO USA
[*]*Corresponding author: john.pellegrino@colorado.edu*

Abstract

We present a methodology and results for measuring crystallization kinetics of sparingly-soluble salt mixtures typical of reject/concentrate streams from membrane-based, inland water supply processes. More usable water can be recovered (and lower disposal costs incurred) from these concentrate streams through efficient crystallization. In this work, we present a steady state, continuous stirred tank reactors (CSTRs)-in-series approach to study crystallization kinetics of a model solution mixture that is supersaturated in $CaCO_3$. We have used pH, conductivity and turbidity changes in the system to monitor crystallization using six CSTRs with individual residence times of nominally 3, 5, and 11 min. This system operates in a steady state mode with total crystallization times from ~ 15-68 min and was capable of handling up to ~0.59 L/min of hard water for the shortest residence time studied. The supersaturation was depleted ~25% and over 50% with total reactor system residence times of ~15 and 68 min, respectively, without any added chemicals. Using the metric of 5 NTU turbidity as being the point of discernible crystal formation, we examined how mixing energy dissipation affects the induction times for crystallization. Notably, discernible crystallization could only be advanced to the 1st CSTR by using a recirculation loop to "fine-tune" the effect of surface area exposure-to-volume ratio, as well as, mixing energy dissipation. A rudimentary, semi-empirical model was used to capture the parametric trends of our experimental results, using the Kolmogorov mixing lengths, surface area-to-volume ratios, flow rates, and nominal diffusion coefficients. This parameterization may be tested further for design scale-up guidance.

1 Introduction

It is well accepted that a major drawback to widespread adoption of reverse osmosis (RO) desalination for inland areas is the lack of economical and environmentally-satisfying solutions for handling the concentrate streams generated from desalination processes[1]. Sparingly-soluble salts from ions such as calcium, barium, strontium, magnesium, and silica, if present, limit the amount of water that may be recovered due to them becoming supersaturated and depositing (scale) on the membrane and other surfaces[2-6]. A number of inclusive reviews[1, 4-12] of concentrate (brine) management methods are available. In many cases, these methods include the controlled crystallization of the supersaturated salts, which brings the solution back to saturation, thus, opening the possibility for further water recovery, and lowering the amount of concentrate for ultimate disposal. Such crystallization (precipitation) processes[3, 13-18] have been examined in prior research studies, with added chemicals and/or seed crystals, but uncertainty remains about scale-up designs (and economic viability). To address this challenge, there are two overarching technical questions: *i*) what are the least expensive (and most efficient) process designs for a crystallizer to bring supersaturated concentrate streams back to saturation, and *ii*) when you have a design idea, how can you best evaluate it on the bench-scale to obtain initial process design metrics for preliminary technoeconomic analysis? This paper presents our development of a methodology to address the latter question by means of obtaining nominal kinetic parameters for preliminary design analysis and quantifying effects of mixing parameters.

We note that there is substantial literature studying scaling on RO membranes during desalination[3, 19]. Among past work are approaches for monitoring scaling using normalized flux decline[20], acoustic reflection signal analysis[21] and visualization techniques[22]. These technologies allow for real-time monitoring of scale formation on membranes and possibly can facilitate the optimization of anti-scaling/fouling interventions. Though these methods offer a way to detect nominal scaling kinetics on membrane surfaces, their usefulness to measure bulk crystallization kinetics are unclear.

Insofar as crystallization process studies are concerned, an exhaustive coverage of prior literature is outside the scope of this work. Rather, in Table 1 we have listed examples of bench-scale, crystallization reactor configurations and studies performed, for both aqueous, sparingly-soluble salt precipitation, as well as, high value compounds, to illustrate the breadth of inquiry that has informed and motivated our current research initiative.

Table 1. Illustrative examples of experimental crystallization process design studies[1]

crystallizing material /composition	configuration	notes	ref.
$CaCO_3$ electrolyte 0.3-1.4 mg/L Ca^{2+}; 0.7-1.3 mg/L HCO_3^-; 8.5-9.6 mg/L Na^+	stainless steel scaling surface in contact with supersaturated solution in steady flow	studying heterogenous nucleation using a well-defined surface under steady flow conditions	[23]
three types of compositions *i*: $CaCl_2.2H_2O$ (1 mol/L) Na_2CO_3 (1 mol/L); *ii*: Na_2SO_4 added as 10 mol% of Na_2CO_3; *iii*: 10 mol% of Na_2CO_3 replaced by Na_2SO_4	batch experiments w/ in-situ small and wide-angle x-ray scattering used to study kinetics and evolving of various polymorphs ACC > dehydrated ACC > vaterite > calcite	sulfate retards vaterite formation and crystal growth kinetics but does not impact ACC stage; sulfate stabilizes vaterite polymorphs	[24]
2 part soln. mix (1) $CaCl_2$ [0.200 mol/L; pH 5.15)] (2) $(NH_4)_2CO_3$ [0.16-0.3 mol/L; pH 12.1-12.2]	batch and SFTR (a modified PFR), crystallizing liquor boluses separated by gas or immiscible liquid to ensure greater degree of plug flow behavior	difference in calcium carbonate polymorphs between batch and SFTR was observed (batch: calcite and vaterite @ 20°C; SFTR: vaterite @ 30°C); xanthan gum addition and changing levels of supersaturation changed presence of vaterite / calcite polymorphs; mixing studied qualitatively—a Y shaped tube to introduce solutions provided less mixing and less crystallization than introducing the reactants through opposing tubes in cross shape	[25]

[1] *ACC* — *amorphous calcium carbonate*
API — *active pharmaceutical intermediate*
COBC — *continuous oscillatory baffled crystallizer*
CSTR — *continuous stirred tank reactor*
FRBM — *focused beam reflectance method*
MSMPR — *mixed-suspension-mixed-product-removal*
PSD — *particle size distribution*
PFR — *plug flow reactor*
RTD — *residence time distribution*
SFTR — *segmented flow tubular reactor*

crystallizing material /composition	configuration	notes	ref.
$CaCl_2$ (2-1000 mmol/L) $(NH_4)_2CO_3$ 0.25-1 g with 20 mL of water to generate CO_2	batch type experiments, $CaCl_2$ solutions of various concentrations exposed to changing partial pressures of CO_2 by varying $(NH_4)_2CO_3$ used to generate CO_2	at low [Ca^{2+}], thermodynamic control limits precipitation; at [Ca^{2+}] > 80 mmol/L the partial pressure of CO_2 influences crystallization; at high partial pressures system is kinetically controlled with vaterite polymorph and vaterite crystallization increases with increasing CO_2 partial pressure	[26]
supersaturated solutions with respect to [$CaCO_3$] 0-0.03 mol/L and [$CaSO_4$] 0-0.03 mol/L equivalents were prepared using $CaCl_2$ & $NaHCO_3$ and Na_2SO_4 (60, 70, 80°C)	batch type	the solubility (when compared to pure salt) of $CaCO_3$ goes through a minimum and then increases with increased sulfate concentration (>0.01 mol/L) but then this effect levels off	[27]
$CaCl_2$ 0.1 mol/L in various alcohols (methanol, ethanol, propanol, butanol and pentanol) [1.75-50 wt% on total soln.]. CO_2 generated from ammonium carbonate and water	batch type, similar to sessile drop method; SEM image analysis with qualitative studies	addition of alcohol leads to thermodynamically controlled preferential calcite polymorph; Hopper crystal formation is kinetically controlled	[28]
2 part solution ($CaCl_2$ and $NaHCO_3$) was between 0.115-0.119 mol/L calcium-to-carbonate activity ratio was 0.99-1.01; pH adjusted to 8.5 using NaOH; Mg^{2+} introduced as $MgCl_2$	flow-through system	Mg^{2+} retards calcite crystallization due to being incorporated in the crystal lattice causing increased solubility of $CaCO_3$	[29]
[$Ca(NO_3)_2$] ~0.0024-0.0032 mol/L [$Ca(NO_3)_2$]:[$NaHCO_3$]=1:1. 10%v/v ethanol and other alcohols. pH adjusted ~8.5 using 0.1 mol/L KOH; solution was maintained at constant supersaturation by tracking pH changes and keeping pH constant by adding $NaHCO_3$, Na_2CO_3 and $Ca(NO_3)_2$	steady supersaturation experiment in a batch reactor	alcohol affects vaterite precipitation, stabilizes unstable vaterite and hinders more thermodynamically stable calcite polymorph.	[30]

crystallizing material /composition	configuration	notes	ref.
$CaCl_2$ and $NaHCO_3$ pH 8.1	batch stirred CSTR	at 150 rpm, all vaterite transformed to calcite in 60 min; at 1000 rpm, vaterite was dominant polymorph; crystal growth is rate limiting step to reach calcite equilibria; addition of polyelectrolyte stabilized vaterite polymorph under slow and fast stirring	[31]
$CaCl_2{\cdot}2H_2O$ and $NaHCO_3$, $[Ca^{2+}]$ = 0.01-0.05 mol/L	batch type with particle vision measurement and FRBM to measure PSD	nucleation and growth take place simultaneously, i.e., number of particles and size of particles increases; growth rate was found to be an exponential function of Ca concentration.	[32]
$CaCl_2$, $NaHCO_3$, 50 mM NaCl, conductivity 7.5 mS/cm pH 6.8-8.1.	flow reactor with an electrochemical setup; once-through flow across cathodic compartment and anodic compartment was in recycle mode; accomplished using a cationic membrane, dimensionally stable electrode and a stainless-steel cathode plate	in $CaCO_3$ precipitation, the electrochemical cell's cathode provides alkalinity i.e. pH on a boundary layer and the cathode surface acts as a scaling surface; by separating anode and cathode layers by an appropriate membrane, the alkaline region is now in the bulk as opposed to a thin layer adhering to the cathode surface.	[33]
$[Ca^{2+}]$ = 0.03 mol/L $[CO_3^-]$ = 0.02-0.03 mol/L $[SO_4^{2-}]$ = 0.02-0.03 mol/L @ 60 and 70 ^{0}C	batch type, 600 h studies	$CaSO_4$ and $CaCO_3$ co-precipitated and $CaSO_4$ precipitated as monoclinic dihydrate; as $CaCO_3$ levels increased $CaSO_4$ formed a more tenacious scale and also the rate of $CaSO_4$ precipitation decreased; CO_3^{2-} may be impacting $CaSO_4$ solubility; increasing precipitation increased co-precipitation rates	[34]
0.5 -1.5 M NaCl, $[CaSO_4]$ = 0.06-0.15 mol/L, $[CaCO_3]$ = 0.007-0.02 mol/L, $[CO_3^-]$:$[SO_4^{2-}]$ ~2-8	batch reactor, membrane pieces added to study the precipitation	increases in NaCl levels increased $CaSO_4$ precipitation but only slightly affected $CaCO_3$ precipitation; membrane-$CaCO_3$ adheres strongly; $CaSO_4$ adheres loosely; $CaSO_4$ adheres strongly in the presence of $CaCO_3$	[35]

crystallizing material /composition	configuration	notes	ref.
$[OH^-]$ = 5-100 mol/m^3 $[CO_2]$ = 4.17 -15 m^3/s; inner cylinder rotating speed = 26 -105 rad/s; $Ca(OH)_2$ soln flow rate x 10^6 = 5 m^3/s; mean residence time = 600 s	Couette -Taylor reactor, modelled as CSTRs-in-series	the flow rate of $Ca(OH)_2$, CO_2, shear stress and excess species influence precipitation; particle growth is retarded by excess species due to their adsorption on crystals; increased shear stresses improve crystallization by enhancing mass transfer and by reducing excess reactant levels	[36]
$CaCl_2$, $NaHCO_3$, ionic strength ~0.111 mol/L, pH adjusted to 8.5 using 0.5 N NaOH	calcite crystal grown on a crystal of Icelandic spar	at low supersaturations growth is due to surface imperfections, only spiral growth seen; as supersaturation increases 2D surface nucleation becomes important	[37]
$[Ca(OH)_2]$ = 1.96-5.66 wt%. $Ca(OH)_2$ slurry flowrate = 20 mL/min; CO_2 flow rate of 25-65 Lph; residence time 25-58 min.	continuous CSTR reactor with ultrasound (240W & 20 kHz) probe intensification	increasing $[Ca(OH)_2]$ increases particle size with and without ultrasound; increase in $Ca(OH)_2$ flow rate decreases particle size; ultrasound reduces particle size across the board; calcite is the dominant polymorph.	[38]
$CaCl_2$, $NaHCO_3$	crystallization under constant supersaturation performed on Icelandic spar under AFM analysis	CO_3^{2-} availability is rate limiting step, surface diffusion controlled mechanism is dominant, cation adsorption on negatively charged surfaces contributes to rapid growth, overall growth of crystal is dependent on rate limiting steps governed by varied crystal orientations	[39]
$[Ca^{2+}]$ = 20 mmol/L $[CO_3^{2-}]$ = 20 mmol/L, mixing $CaCl_2$, Na_2CO_3 and $NaHCO_3$, pH-controlled addition of NaOH.	single CSTR to study effect of anti-scalant, anti-scalant and supersaturated solution fed continuously	Unsteady state diffusion model could relate anti-scalant adsorption behavior on $CaCO_3$ and scaling inhibition. Increased residence time can greatly reduce precipitation, i.e., longer the residence time more the anti-scalant adsorbs on the $CaCO_3$ particle	[40]
glycine (API)	cooling crystallization using MSMPR in cascade operated in periodic flow mode; not ideal steady flow	controlling crystal properties using RTD	[41]

crystallizing material /composition	configuration	notes	ref.
acetaminophen (API)	PFR with recycle under isothermal conditions	controlling crystal size by manipulating recycle ratio and axial position of crystal extraction	[42]
unknown API (Astra-Zeneca)	cooling crystallization in COBC	system applies a forcing function on plug flow; using *Re* and *St* as design parameters	[43]
ketoconazole, fluefenamic acid, glutamic acid (levo) (API)	anti-solvent crystallization using PFR with a static mixer	model developed to correlate crystal size distribution to a dispersion based residence time distribution study	[44]
benzoic acid (API)	COBC continuous spherical crystallization	continuous spherical crystallization obtained by altering mixing through manipulation of flow oscillation; *Re* and *St* as design parameters	[45]
cyclosporine	MSMPR in series with recycle with dynamic temperature control.	kinetic model with experimentally determined rate constants for nucleation and crystal growth in terms of crystal size and mass correlation	[46]
asparagine monohydrate (levo)	PFR with gas-liquid hydrodynamic induced slug flow	tight control of RTD by separating slugs by inert gas to ensure good control of crystal size distribution.	[47]

It is important to note that fundamental studies on sparingly-soluble salt crystallization have most often involved a batch process operating at unsteady state[48-52]. For example, Rosa and Lundagrer Madsen[48] studied the kinetics of calcium carbonate precipitation from a supersaturated solution formed by mixing calcium chloride and sodium carbonate solutions. They performed experiments in a test tube using pH as a metric to track kinetic changes and classified the crystal morphology at different temperatures for spontaneous crystallization processes. Their results[48] indicated that at 25°C spontaneous crystallization yielded vaterite, calcite at 30°C and aragonite at 37°C. Notwithstanding, Plummer and Busenberg[52] also studied the solubility of aragonite, vaterite and calcite and their research showed calcite was the most stable and vaterite the least. Thus, whereas thermodynamics may dictate the most stable polymorph at equilibrium, the study of kinetics may not be restricted to only one polymorph of the crystal, which follows from Ostwald's observation that the first crystal polymorph to appear is likely the most unstable[53]. Thus, besides actual depletion of calcium in the form of $CaCO_3$

the transition in morphology adds another layer of complexity in the study of crystallization kinetics, which we are not explicitly including in our current studies.

Batch reactor crystallization of gypsum, another sparingly-soluble salt, was done to elucidate the effect of sand particles as seed materials for promoting crystallization kinetics[18]. In this case, as well as others, ions such a magnesium were not present. The absence of ions such as magnesium and sulfate combined with small volumes of solution makes comparison of bench-scale results to large scale processes more uncertain[48]. In addition, it is important to consider that using the titration of calcium ions as a metric to measure $CaSO_4$ (gypsum) crystallization kinetics, especially with EDTA (ethylenediaminetetraacetic acid)-based methods[18], can have more artifacts when studying compositions that include divalent cations other than calcium[54].

Another approach to measure the induction time for crystallization is cryo-TEM[55], which was used to posit the theory of formation of amorphous calcium carbonate (ACC) during the induction stage[56, 57]. The drawback of techniques that use complex instrumentation such as TEM is that they cannot be used in analyzing larger, more complex bench-scale processes, such as the approach we will be describing.

Crystallization kinetics observed in batch reactors may not be indicative of kinetic processes observed in flow reactors that are desirable at industrial scale. Researchers have recently studied the effects of agitation i.e. mixing on induction time for nucleation[58] and the mixing characteristics of flow reactors are considerably different from that of batch reactors. For example, Liu et al.[58] developed correlating parameters relating agitation and crystallization of butyl paraben and m-hydroxybenzoic acid. They concluded that the nucleation rate increases with the energy dissipation rate to the power 0.45. They also found that specific nuances in the way locally-high shear rates could be developed will influence the induction time (inversely proportional to the nucleation rate).

Swinny et al.[59] used a mixed-suspension-mixed-product-removal (MSMPR) crystallizer to study crystallization kinetics of calcium carbonate using a population balance model. They observed morphology changes for different reactor residence times, for example, aragonite and calcite were the dominant morphologies at lower (225 ppm) and higher (350 ppm) levels of calcium concentration, respectively, and a transition from aragonite to calcite was observed as the level of initial supersaturation was increased. The depletion in supersaturation was between

74 and 90%. Zhu et al.[60] have also discussed an MSMPR system to study $CaCO_3$ precipitation kinetics combined with a population balance model to study nucleation, agglomeration and crystal growth. Nonetheless, techniques that use a population number model or a crystal size growth-based kinetic measurement are highly instrument-intensive and less facile for early process scoping. To evaluate procedures that can be applied to enhance crystallization, a robust method to assess crystallization kinetics is desirable. Though the use of an MSMPR, a continuous reactor, does provide kinetic analysis more closely akin to scaled-up processes, than a batch reactor, the use of a single MSMPR isolates the crystallizing solution corresponding to only one particular age and supersaturation characterized by the single residence time used.

Therefore, there is a justification to develop techniques to study the crystallization kinetics of sparingly-soluble salts that can provide adequate scale-up design information to aid in technoeconomic analysis for large scale systems associated with water production. In this study, we have demonstrated a steady state, continuous stirred tank reactors (CSTRs)-in-series system that offers a more facile method for kinetic analysis over multiple residence times within the crystallizing system. This methodology also allows for a better approximation (and sensitivity to process variables) for the induction time. We present results for crystallization of $CaCO_3$ from a model, complex, supersaturated solution created by mixing two unsaturated electrolyte solutions together. We used turbidity[61] as the key metric to quantify crystallization, as well as, collecting precipitate and analyzing supernatant ion concentrations, to quantify the overall $CaCO_3$ material balance. We examine the effects of the residence time in each of the six CSTRs-in-series and the specific energy (mixing) dissipation on the apparent induction time for nucleation and the overall depletion of supersaturation. The uniqueness of our contribution is twofold, firstly devising a steady state CSTRs-in-series experimental approach to study crystallization kinetics and secondly, formulating an initial semi-empirical approach for quantifying scale-up parameters in terms of Kolmogorov mixing lengths and other process-specific variables.

2 Methods

2.1 Sampling and measurements

An Ecosense™ EC300 meter was used to measure conductivity and a Oakton pH 100 Series was used to measure pH. Turbidity measurements were taken by extracting a sample of ~15 mL from the reactor in a cuvette and analyzing it in a Hatch™ 2100Q turbidimeter compatible with EPA method 180.1 (detection normal to incident light). The solution in the cuvette was discarded after measurement.

2.2 Crystallization using CSTRs-in-series

The experimental setup incorporates a Philips and Bird™ impeller fixture (including six impellers) and a set of six acrylic jars. Masterflex™ peristaltic pumps equipped with appropriate tubing (as per required flowrate) were used to transfer the crystallizing solution from one CSTR to another. The volume in each CSTR (V_0) was maintained using a dynamic weir system. The suction ends of the tubing were placed at a specified height from the base of the tank such that the pumps remove and transfer the liquid only when the set volume has been reached in it. Solutions 1 and 2 (each at x mL/min) were also transferred into the first reactor using separate peristaltic pumps. The residence time in each CSTR was then defined as $\tau = V_0/2x$.

A schematic of the apparatus is shown in Figure 1 and an example of the development of turbidity across the CSTRs-in-series is shown in Figure 2. Turbidity, conductivity and pH measurements were taken after the CSTRs-in-series system reached steady state; that is, after the final CSTR's operating time exceeded the estimated stabilization time, t_s (this will be discussed in the subsection 2.2.1).

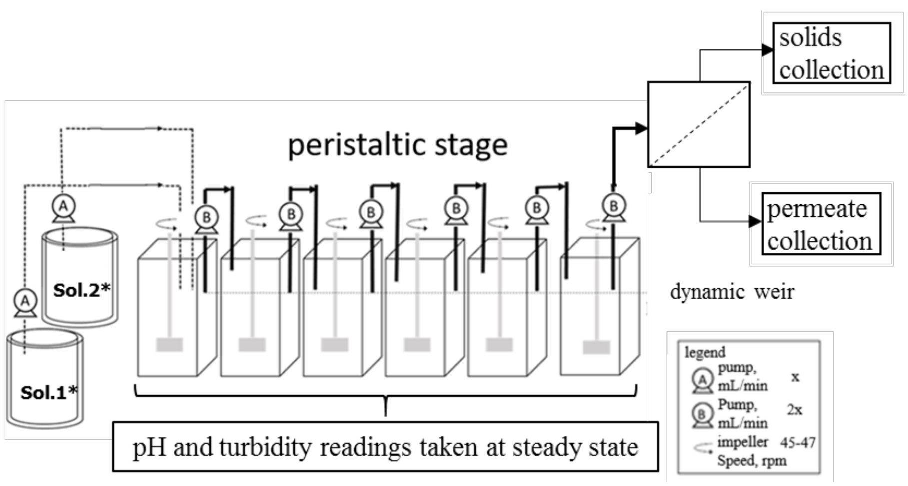

Figure 1. Schematic representation of CSTRs-in-series setup.

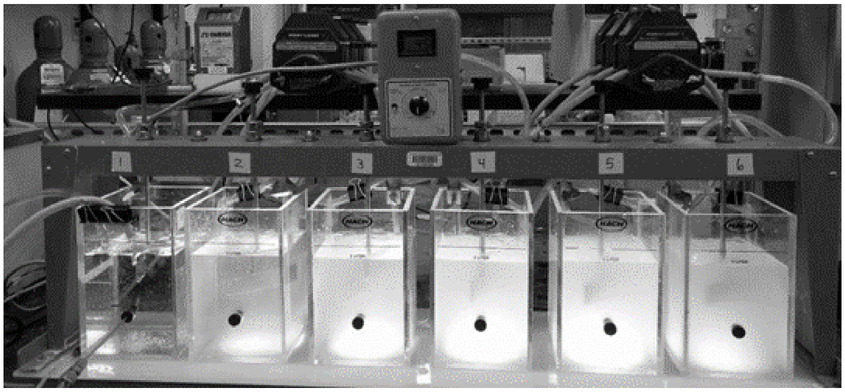

Figure 2. Six CSTRs-in-series running at steady state (τ~11 min). Observe the increase in turbidity from left to right.

Crystallization experiments were primarily done for three nominal CSTR residence times of 3, 5, and 11 min (with a few additional ones to address specific questions). Table 2 presents some relevant system metrics associated with these CSTRs-in-series experiments. The final column includes the nominal surface area-to-volumetric flow ratio since crystallization kinetics are expected to include surface interactions. During baseline experiments, the impeller speed was set at ~45 rpm. More details on mixing will be discussed in subsequent sections.

Table 2. Nominal CSTR metrics during crystallization experiments

nominal residence time (τ) in each CSTR, min	**CSTR volume, m^3 x 10^3**	**wetted CSTR surface area (A_T), m^2 x 10^2**	**volumetric flow rate (q_o), m^3/s x 10^6**	**A_T/q_o, s/m x 10^4**
3	1.75	7.43	9.74	0.8
5	1.75	7.43	5.83	1.3
11	1.75	7.43	2.66	2.8

2.2.1 Modeling CSTR start-up

To guide experimental operating procedures, we estimated when the system may reach steady state after startup. We empirically considered the kinetics to be first order, with rate constant *k*, and assumed the CSTRs to be ideal with an average residence time, τ. Using the unsteady-state analysis of a CSTR[62], and defining the stabilization time (t_s) as being when the concentration is 99% of its final steady state value, then

$$t_s = \frac{4.6\,\tau}{1+\tau k}, \qquad (1)$$

and for a slow reaction rate constant, k, $t_s = 4.6\tau$. Note, as k increases t_s decreases, thus, we can safely estimate that steady state is achieved by waiting at least 5τ for any CSTR. This was experimentally confirmed during screening experiments not included in this manuscript.

2.2.2 Modeling mixing effects

Our baseline experimental set-up contained two sources of mixing after introduction of the two electrolyte solutions into the 1st CSTR. Each CSTR has a stirring impeller, and between each CSTR we used peristaltic pumps to transfer the solution and maintain the dynamic weir.

Peristaltic pumping involves subjecting a flexible tubing to a sinusoidal forcing wave and the consequent crests and troughs generated allow for fluid transport, including secondary flows (eddies)[63]. For our purposes, these secondary flows likely contribute to mixing thereby helping overcome rate limiting mass transfer resistances in the crystal nucleation and growth process.

Even though the fluid dynamics of peristaltic pumping are complex, and beyond the purview of this paper, we wish to include (and compare) it on a somewhat equivalent basis with the impeller agitation, so our approach involved simple methods of estimating the power consumption and subsequent energy dissipation for each type of mixing, followed by estimation of the Kolmogorov mixing length scale[64]. We note that a dynamic weir may cause periodic two-phase (slug flow), which can complicate the calculation of a mixing length scale due to energy injection from any recirculation regions within the tubing[25, 47], but we have ignored this effect at this time.

The Kolmogorov mixing theory envisages that the macroscale eddies cause mixing through constant energy dissipation resulting in smaller and smaller eddies which then ultimately reach a very small scale where turbulence is universal, i.e. at the Kolmogorov scale all eddies have the same characteristics. This universal scale can be estimated using dimensional analysis. Kolmogorov scales depend only on energy dissipation and the kinematic viscosity (ν) of the process fluid. The Kolmogorov mixing length was calculated by the expression[65]:

$$\eta = \left(\frac{\nu^3}{\varepsilon_{tot}} \right)^{1/4} \tag{2}$$

where ε is the total mixing energy that is dissipated into any system volume.

For peristaltic pumping, initially we simply used the work to overcome friction in the tubing as the power dissipation associated with the pumping action and did not include any flow peculiarities that may be associated with the specific compression and expansion of the tubing. (Note, this was later modified in our empirical model fitting, which will be discussed in the Results.) The tubing inside diameter and length between each CSTR was 7.9 mm and 1.2 m, respectively. Across all residence times the flow in the tubing was assumed laminar. The total pressure drop in the tubing was obtained using the Darcy-Weisbach equation[66].

$$\frac{\Delta p}{L} = \frac{\rho}{2} f_D \frac{u_{avg}^2}{D} \tag{3}$$

Where Δp is the total pressure drop along length of the tubing (L); the crystallizing liquor's density, ρ (and viscosity) were estimated using the OLI Stream Analyzer[67]; u_{avg} is the average velocity of fluid in the tube; D is the inside diameter of the tube; and the Darcy friction factor f_D can be calculated by the empirical relationship between the friction factor (f_D) and Reynolds number (Re).

$$f_D = \frac{64}{\mathrm{Re}} \tag{4}$$

Power dissipated due to flow in tube (P_{tube}) is obtained by using the pressure drop of the fluid (Δp) in transport and the volumetric flow rate (q).

$$P_{tube} = \Delta p \times q \tag{5}$$

Thus, the energy dissipation during the pumping action inside the tube (ε_{pump}) is given by,

$$\varepsilon_{pump} = \frac{P_{tube}}{m_{tube}} \tag{6}$$

m_{tube} refers to the control mass of crystallizing liquor in each tubing stage (~59 mL) preceding each CSTR. To estimate the power associated with impeller agitation, we calculated the Newton number (N_p) using the empirical formulations developed by Furukawa et al.[68]. The power associated with the impeller (P_{Im}) is given by the expression:

$$P_{Im} = N_p \rho N^3 D_{Im} \tag{7}$$

where, N is impeller rotation speed in s^{-1}, and D_{Im} is the diameter of the impeller. Similarly, as above, the energy dissipation of the impeller can be calculated as $\varepsilon_{Im} = P_{Im}/m_{CSTR}$ (where m_{CSTR} is the mass of solution in the CSTR).

Power dissipated due to the momentum of fluid entering the CSTR (P_k) is given by

$$P_k = \frac{1}{2}\rho q u_{avg} . \tag{8}$$

Note, for the 1st CSTR the feed enters through 2 tubes each with a flow rate of $q/2$.

Dissipation due to fluid momentum in each CSTR (ε_k) is given by

$$\varepsilon_k = P_k / m_{\mathrm{CSTR}} . \tag{9}$$

Therefore, bulk energy dissipation in a tank is given by $\varepsilon_{bulk} = \varepsilon_{Im} + \varepsilon_k$.

2.2.3 Collection of crystal precipitate

For several experiments, the suspended crystal precipitate was collected from the final CSTR after the system reached steady-state. About 1.3 to 1.8 L of liquor from the 6th CSTR in the CSTRs-in-series reactor configuration was pumped through a 0.2 µm ePTFE filter (Donaldson AX09-059, pre-wetted by isopropanol) encased in an acrylic membrane crossflow cell but used in normal (dead-end) filtration mode. This filtration took ~10 min. The permeate was carefully collected in a vessel connected to a vacuum. The membrane was pre-weighed after drying. The membrane with the $CaCO_3$ precipitate was dried overnight and the mass of the membrane and precipitate was measured and thus the mass of $CaCO_3$ per L of permeate was ascertained. Some of the selected permeate streams were also sent for ICP-OES/or MS (inductively coupled plasma optical emission spectrometry/or mass spectroscopy) analysis to measure the concentration of Mg^{2+} and Ca^{2+} ions.

The mass balance over calcium is obtained as $[\mathrm{Ca}^{2+}_{\mathrm{inlet}}] = [\mathrm{Ca}^{2+}_{\mathrm{permeate}}] + [\mathrm{Ca}^{2+}_{\mathrm{precipitate}}]$. In the case of suspended precipitate collection, $[\mathrm{Ca}^{2+}_{\mathrm{precipitate}}]$ is determined by direct precipitate collection and in the case of ICP-OES $[\mathrm{Ca}^{2+}_{\mathrm{permeate}}]$ is known and then $[\mathrm{Ca}^{2+}_{\mathrm{precipitate}}]$ can be calculated using the known inlet concentration of calcium ions. As per our solution preparation scheme, $[\mathrm{Ca}^{2+}_{\mathrm{inlet}}]$~532 ppm (mg/L) and in the temperature range of the experiments conducted

(~20-24°C), the amount of $CaCO_3$ precipitate theoretically predicted at equilibrium is ~470 ppm (0.47 g/L) (see Figure 3).

2.2.4 Mixing using peristaltic pumping recirculation

To assess the effect of peristaltic pumping on nucleation in the initial CSTR of the crystallization, a separate set of experiments were performed with recirculation-based mixing carried out only in that CSTR using a peristaltic pump. These experiments used a pump similar to those used to transfer liquid from one CSTR to another. However, this pump merely recirculated the liquor in the 1st CSTR of the series setup. The crystallization process was allowed to reach steady state without this recirculation; measurements of turbidity, conductivity and pH were taken, and then the recirculation was started. Once again, the system was allowed to reach steady state and the same measurements (with an ~30 min lapse in between) were taken. Permeate and precipitate from the 6th CSTR were also collected. These experiments were conducted with several average CSTR residence times (note, the additional fluid volume in the recirculation tubing was included when calculating the actual residence time) and different recirculation rates.

2.3 Electrolyte solution

We used a model water composition based on a water desalination pilot project done in Brighton, CO (see Table 3).

Table 3. Brighton water quality analysis for model water.

parameter		raw water - Brighton, CO
calcium	mg/L	107
magnesium	mg/L	24
sodium	mg/L	121
chloride	mg/L	125
sulfate	mg/L	213
bicarbonate	mg/L	179
silica	mg/L	19
pH		7.02
T	°F	62

An initial water recipe (see Table 4) based on mixing together Na2SO4, NaHCO3 and CaCl2, with the other constituents—SiO2 was eliminated due to difficulty getting it solubilized, which would result in artifacts from variable seed particles—has been determined, using OLI Stream Analyzer[67] software and trial-and-error calculations, to rationalize the main water quality composition from this Brighton water quality analysis. The mixture equilibrates to a supersaturated solution with respect to CaCO3. The rapid mixing of this mixture into the 1st CSTR tank allows us to unambiguously set the initial time, t = 0, for the crystallization rate measurements.

Table 4. Model electrolyte solutions mixed to achieve supersaturation.

species	solution 1	solution 2
water	500 g	500 g
calcium chloride ($CaCl_2$)	1.4760 g	
magnesium sulfate heptahydrate ($MgSO_4 \cdot 7H_2O$)	1.2078 g	
sodium sulfate (Na_2SO_4)		1.5624 g
sodium bicarbonate ($NaHCO_3$)		1.5624 g

According to the equilibrium calculation (using OLI Stream Analyzer)[67], at 22°C and 85 kPa (the nominal conditions in our lab) this mixture equilibrates with 0.4684 g of calcite ($CaCO_3$) precipitate. Its conductivity would be 5.448 mS/cm. As shown in Figure 3, between 18-28°C, the conductivity varies from 4.985-6.157 mS/cm, so temperature can make a significant difference in this variable. Solutes precipitated varies from 0.4665 to 0.4727 g/L in this same temperature range.

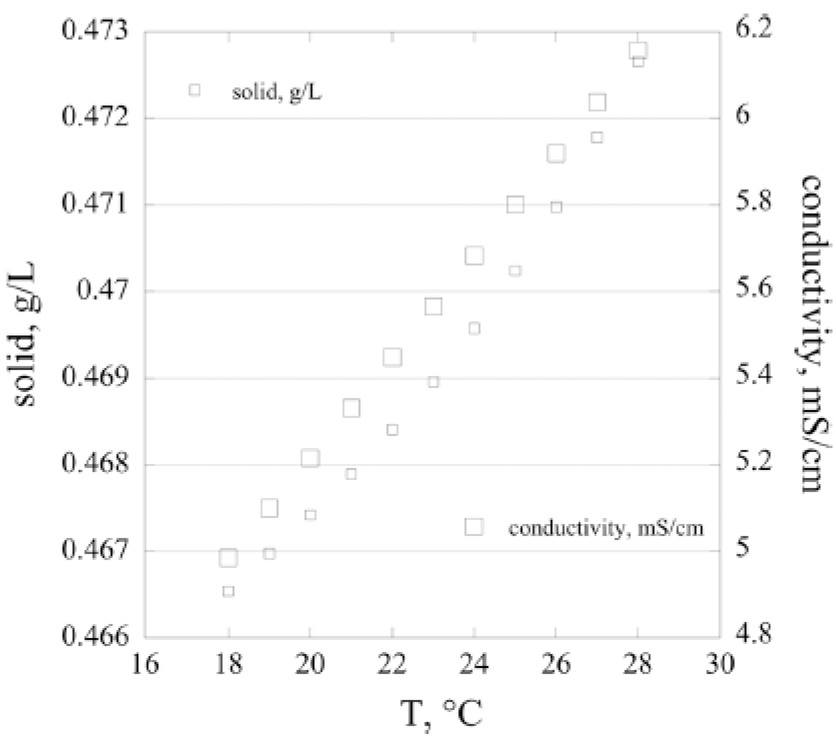

Figure 3. Estimated calcite precipitated and solution specific conductivity at equilibrium for the mixed composition from Table 4.

3 Results and discussion

3.1 Baseline turbidity, pH, and conductivity responses

Conductivity did not provide adequate resolution to track the kinetic changes in the system. Though pH measurements showed a constant decline as crystallization proceeds (Figure 4), reflecting a decrease in CO_3^{2-} alkalinity, the absolute spread of pH values varied significantly (between ~0.5 pH units) across replicates. Nevertheless, the consistent trend of declining pH (implying decreasing alkalinity) reinforces credibility for using the turbidity metrics (Figure 5) for crystallization kinetics across the CSTRs-in-series. It was observed that the turbidity values consistently increased across reactors for all experiments. A similar approach of using turbidity as a metric to study crystallization was used by Shih et al.[69].

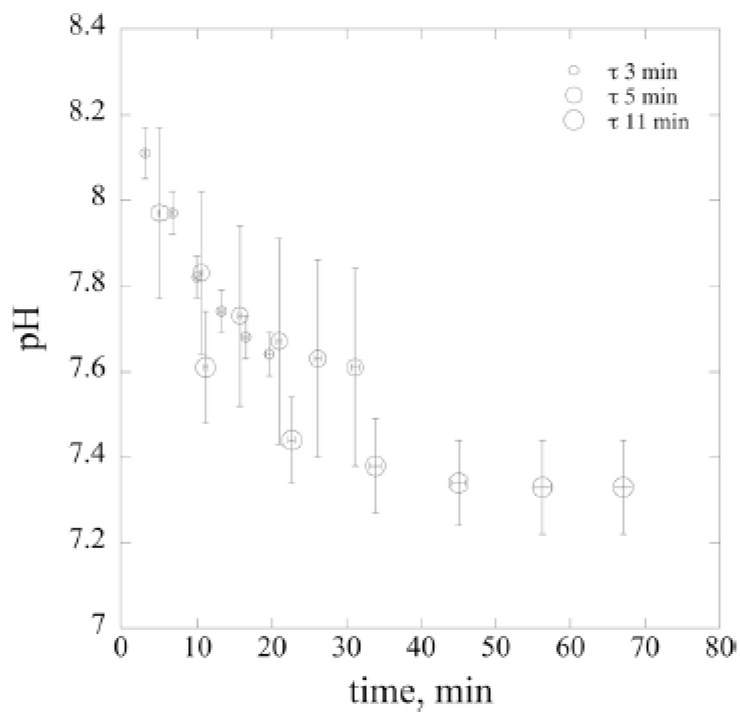

Figure 4. pH vs. reaction time (min). Each data point is a CSTR (nos. 1-6 left to right) for the particular residence time, τ. The uncertainties are 1 standard deviation.

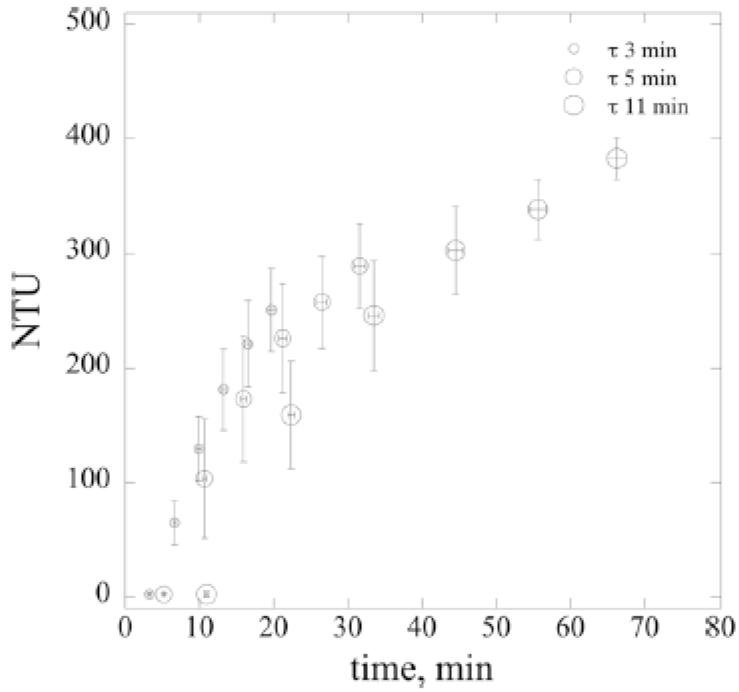

Figure 5. Turbidity (NTU) vs. reaction time (min). Each data point is a CSTR (nos. 1-6 left to right) for the particular residence time, τ. The uncertainties are 1 standard deviation.

Notwithstanding this consistency, turbidity measurements are affected by the number density of particulates, and their optical characteristics, size, and morphology, which makes their use for quantitative analysis of the system's depletion in calcium supersaturation challenging. While a more straightforward way to track depletion of calcium ions is often to use a calcium ISE (ion selective electrode probe), the interference of magnesium ions in the crystallizing liquor, and degradation of the membrane sensing system[69], makes such an approach problematic. Thus, we have also obtained mass balances to provide a correlation between the turbidity in the 6th CSTR and depletion of Ca ion supersaturation. Table 5 presents the mass of solids precipitated and depletion of supersaturation, with respect to the theoretical solid precipitation at equilibrium (see Figure 3), both in terms of suspended precipitate collection and mass of precipitate obtained from ICP-OES data (in $CaCO_3$ equivalents).

The depletion of supersaturation is higher when calculated from the ICP-OES results as compared to direct precipitate collection. This is explainable by the observation that some amount of precipitate settles at the bottom, and scales on the sides, of the CSTRs. Thus, the ‘recovery’ of precipitate from the mixed liquor through filtration would exclude these crystals.

Table 5. $CaCO_3$ precipitated

residence time, τ (min)	$CaCO_3$ precipitated (g/L) [solids collected]	$CaCO_3$ precipitated (g/L) [ICP-OES]	% depletion of supersaturation using solids collected	% depletion of supersaturation using ICP-OES	note
3 ± 0.4	0.13	0.19	27.8	41.1	(i)
5 ± 0.4	0.17	0.23	35.7	49.8	(ii)
11 ± 0.5	0.24	0.31	50.9	66.4	(iii)

(i) average of 3 experiments ICP-OES; average of 7 experiments precipitate collection
(ii) average of 3 experiments ICP-OES; average of 8 experiments precipitate collection
(iii) average of 4 experiments ICP-OES; average of 7 experiments precipitate collection

It is reasonable to expect more total crystallization with longer overall reaction times, i.e. residence times. Interestingly, since crystallization is a surface dependent phenomenon, thus, besides residence time, the surface area of each reactor exposed may also be an important factor, as noted by Liu et al.[58] The walls of the reactors could act as nucleation sites, thereby increasing the rate of crystallization. Figure 5 shows increasing turbidity with respect to reaction time and the CSTR-in-series. Since the nominal slope of turbidity vs. time was steeper for the lower τ values (Figure 5), homogeneous bulk crystallization may not be the sole determiner for our kinetics measurements.

3.2 Mixing influences on crystallization kinetics

It is noteworthy that for all of our experimental residence times visually discernible crystallization (NTU > 5, our subjective assessment) <u>was only observed</u> in the 2nd CSTR of the series configuration. This observation stimulated our hypothesis that the peristaltic pumping between tanks affects crystal nucleation/formation. Table 6 provides an order of magnitude estimate of energy dissipation for both the pumping (ε_{tube}) and impeller (ε_{Im}) mixing actions (using the procedures discussed in sections 2.2.2 and 3.3). It can be observed that ε_{tube} values are 1-2 orders of magnitude above that of ε_{Im} confirming that impeller action at 45 rpm may have significantly less mixing effectiveness than the interstage pumping. Thus, the higher slopes of turbidity change (see Figure 5) at lower τ values (i.e., higher ε_{tube}) could be explained by higher mixing energy dissipation in reactors 2-6 in such cases (sum of last three columns in Table 6).

Whereas, in the 1st CSTR, the energy dissipation is only the sum of the kinetic energy dissipation (ε_k) and ε_{Im}.

Table 6. Energy dissipation from stirring (@45 rpm) and when pumping between CSTRs

τ, min	tube flow rate (q), m^3/s x10^6	u_{avg}, m/s	Re	Δp, Pa	flow power (P_f) $kg{\cdot}m^2{\cdot}s^{-3}$ x 10^5	kinetic power (P_k) $kg{\cdot}m^2{\cdot}s^{-3}$ x 10^5	energy dissipation, $m^2{\cdot}s^{-3}$ ε_k x 10^3	ε_{tube}* x 10^3	ε_{Im} x 10^3
3	9.72	0.2	1537	125	121	19.2	0.109	20.6	0.21
5	5.83	0.12	922	75	44	4.1	0.024	7.4	0.21
11	2.65	0.05	419	34	9	0.39	0.002	1.5	0.21

*Note, ε_{tube} is not relevant for the flow into the 1st CSTR as the crystallizing liquids are pumped in as separate solutions.

3.2.1 Impact of increasing impeller speed in the CSTRs

Besides changing the average residence times, we studied the effect of impeller speed on crystallization. Our rationale was that increased impeller speed would also increase mixing, and thus encourage crystallization. In these experiments, nominal impeller speeds of 92 and 132 (±2) rpm were also used (besides the baseline 45±2 rpm) with nominal residence times of ~3 and 11 min. An impeller speed of 132 rpm proved to be the highest that retained a level-enough liquid surface for the dynamic weir to maintain level control in the CSTRs.

From Figure 6, it can be observed that for impeller speeds of 45 and 92 rpm, turbidity levels for the first 5 CSTRs are comparable though an increased turbidity can be observed at the 6th CSTR for the higher rpm. Nonetheless, the key observation is that turbidity levels at 132 rpm impeller mixing are significantly lower than that for 45 and 92 rpm stirring. This is counterintuitive to the notion that increased turbidity always implies increased crystallization.

It is important to note that turbidity depends on particle size, geometry and optical properties of suspended solid besides their number density. Kleizen et al.[70] had inferred from experiments and modeling that the extent of light scattering in turbidimetric measurements is inversely proportional to particle size, thus turbidity measurements would be higher for smaller particulates with the same number density. Drawing from this idea, the trends observed in Figure 6 may be attributed to changing crystal morphology/size due to the varying impeller speeds. Increased impeller speeds could promote crystal aggregation thereby increasing particle size consequently leading to lower turbidity measurements. There is also the possibility of larger aggregates settling more rapidly to the bottom of the CSTRs and lowering the measured turbidity values. Therefore, a possibility exists where there could be an increased level of demineralization of the crystallizing liquor without turbidity levels increasing (but rather decreasing).

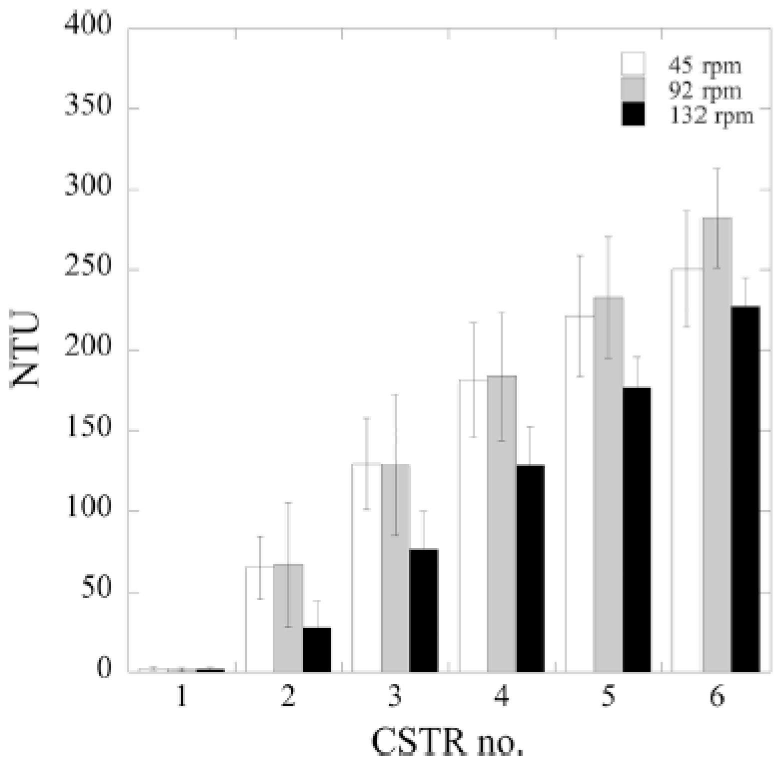

Figure 6. Effect of impeller speeds on turbidity evolution (τ ~3 min).

The precipitate collected from 6th CSTR does not monotonically increase with impeller mixing rpm. The average precipitate collected, from 6-9 experiments for each mixing rpm, was 0.13 (±0.02), 0.17 (±0.01), 0.15 (±0.02) g/L for 45, 92, and 132 rpm impeller speeds, respectively. These data may also point to a possibility of solids settling to the bottom of the CSTRs during our experiments, which we qualitatively observed. Unfortunately, the samples of permeate (during precipitated solids collection) were incorrectly analyzed in the ICP-OES measurements, so we don't have secondary mass balance data to compare to the precipitate collection data.

A third possible rationale for the trends in Figure 6 is that increased mechanical agitation does not always increase nucleation and may, in fact, lower it. Early studies by Mullin and Raven[71] suggested that mechanical attrition occurred which brought crystals below the critical size needed to resist dissolution. Other research[72] has also suggested that there can be a plateau mixing intensity, above which no further benefit to crystallization kinetics are observed.

Notwithstanding these inconclusive results, regarding how the turbidity changes with overall reaction time and impeller rpm, significantly, we still noted that discernible crystallization (turbidity >5 NTU) was not observed in the 1st CSTR even at the higher impeller speeds of 92 and 132 rpm (see Figure 6). Thus, we turned our attention to determining the level and type of mixing that would bring about discernible crystallization (turbidity >5 NTU) in the 1st CSTR as opposed to measuring exhaustion of supersaturation over all 6 CSTRs-in-series.

3.2.2 Recirculation mixing in the 1st CSTR

After start-up of an experiment, with the impeller rotating at 45 rpm (the baseline value), when steady-state was reached, and after data was taken, peristaltic pump-based recirculation was introduced in the 1st CSTR—note, this recirculation flow could not experience two-phase flow because both ends of tubing were always below the fluid surface—and the impeller rotation was maintained. A new steady-state was allowed to be reached, and new measurements of pH, conductivity, and turbidity were taken. Initially, recirculation rates were varied between ~20 - 380 mL/min for $\tau \sim 3$ min and we found that there appeared to be a direct, though nonlinear, dependence of turbidity on the rate of recirculation. Additionally, at 30 mL/min recirculation rate turbidity levels ≥5 NTU occurred.

Similar experimental protocols were then performed for τ's of 5 and 11 min with one recirculation rate in the 1st CSTR set at 380 mL/min. Figure 7 shows that turbidity always increases across successive CSTRs (with higher levels at higher τ's) but only in the presence of recirculation mixing does visible turbidity (≥5 NTU) occur in the 1st CSTR. Additionally, the 1st CSTR's turbidity actually increases by more than an order of magnitude between increasing τ's at this level of recirculation mixing.

The effect on precipitate recovery in the 6th CSTR due to recirculation in the 1st CSTR is shown in Figure 8. The trendline shows the estimate of precipitate collection in the absence of recirculation.

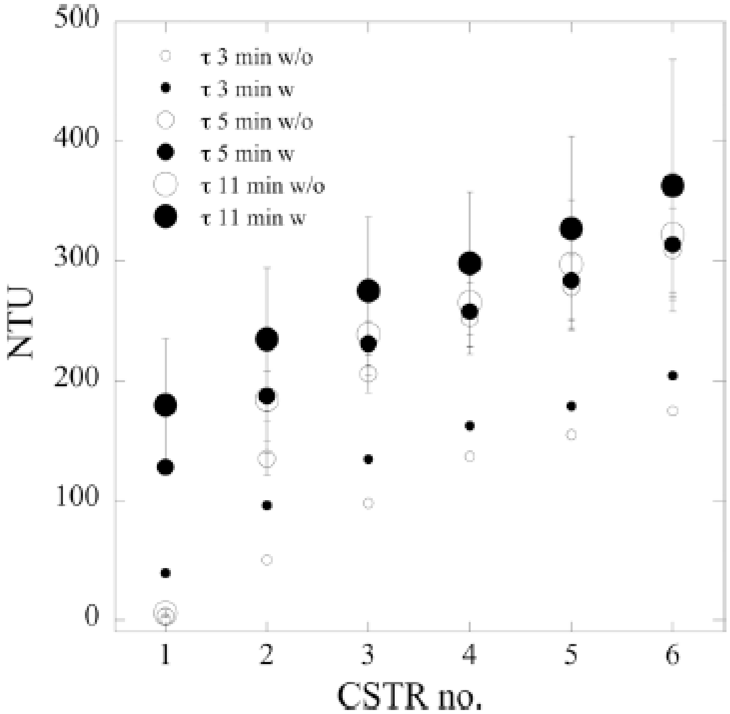

Figure 7. Turbidity vs CSTR no. without (w/o) and with (w) recirculation mixing (380 mL/min) in the 1st CSTR at three residence times (τ). The uncertainties are 1 standard deviation (only one experiment was performed at τ ~3 min).

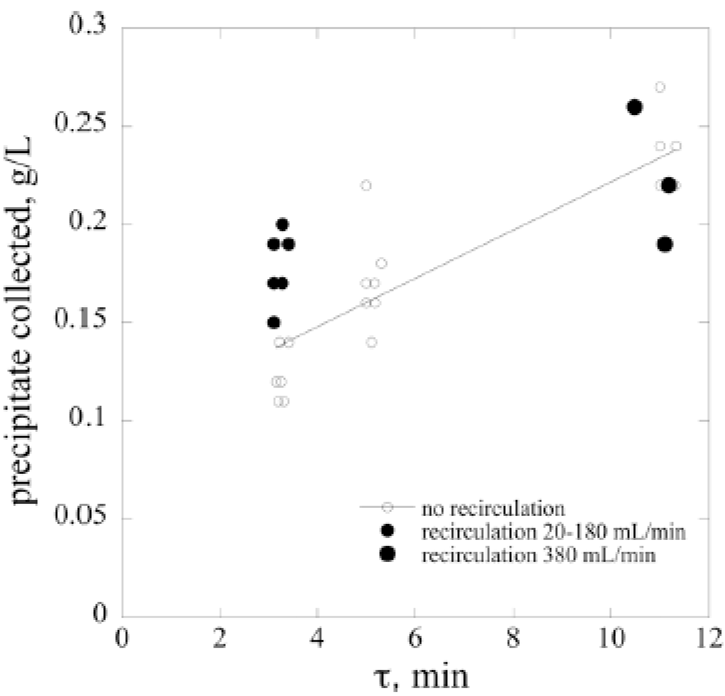

Figure 8. $CaCO_3$ precipitate collected from 6th CSTR vs. residence time with and without recirculation mixing in the 1st CSTR. Trendline presented for the impeller mixing-only data.

3.2.3 Further studies on recirculation mixing in a single CSTR

We adopted a protocol, using just one CSTR, which would elucidate if any synergies between the impeller action and recirculation mixing occurred. Two new types of experiments were performed: recirculation mixing with and without impeller action. In both of these types of experiments τ was ~3 min, and when the impeller was on, it was set at ~45 rpm. The recirculation mixing was started as soon as the CSTR filled up, and then readings of turbidity, pH, and k were taken after ~5τ = 15 min. The recirculation mixing was varied between 10-380 mL/min. The level in this CSTR was still maintained using the dynamic weir system as previously described but was discarded without maintaining further CSTRs-in-series. The turbidity results are shown in Figure 9 and indicate no significant difference between recirculation in conjunction with or without impeller mixing. This further suggests that impeller mixing has little effect on initial formation of discernible crystals in the 1st CSTR.

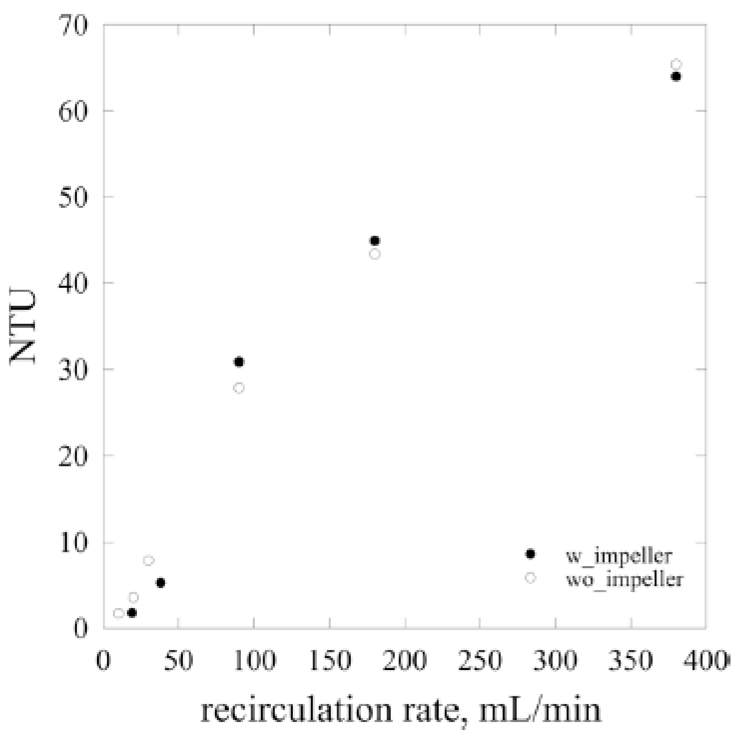

Figure 9. Turbidity in one CSTR using peristaltic-pump-based recirculation mixing with and without additional impeller mixing (@ ~45 rpm) with τ ~3 min.

3.3 Modeling mixing effects in 1st CSTR

The aforementioned experiments using a single CSTR with the three types of mixing: (1) only impeller mixing; (2) only recirculation mixing; and (3) impeller and recirculation mixing (listed in Table 7), were used to quantitatively rationalize the effects from our experimental variables on the apparent crystallization nucleation (aka the turbidity in the 1st CSTR). We created an empirical, mass-action type, rate expression (equation 10) for the initial crystal formation (number density). The expression assumes that the kinetic time scale is controlled by mass transfer and the formation rate of crystal nuclei in different mass transfer environments are additive. First, we write the expression for the bulk crystallization, excluding any surface-related kinetics, and then, we assume that this bulk rate is enhanced by the presence of surface(s)—the inside of the recirculation tubing and the tank's surface—in an additive fashion. The nomenclature, variables, and constant parameters are listed in Table 8.

$$\frac{dN_n}{dt} = k_0 \frac{D_x}{\eta_0^2} C_A^* C_C^* \left[1 + \frac{\eta_0^2}{D_x} \frac{1}{\eta_B^2} q_B S V_B \frac{k_B}{k_0} \phi_{S,B} + \frac{\eta_0^2}{D_x} \frac{1}{\eta_0^2} q_{tot} S V_T \frac{k_T}{k_0} \phi_{S,T} \right] \tag{10}$$

The term outside the square brackets (on the RHS) is the simple, mass action, bulk crystallization rate, excluding any surface-related kinetics, and assumes the time-scale is governed by diffusion through the Kolmagorov length scale for associating ions to meet. Within the brackets there are two rate enhancements due to collisions with surface(s), the first is the walls of tubing during the recirculation mixing and the second represents collisions with the walls of the tank. These rate enhancement expressions resulted from our ad-hoc reasoning and a dimensional analysis approach to create a non-dimensional group which captured the number of possible collisions with favorable surface area "sites" per unit volume and time. For example, in the tubing, the entire volume of fluid has a changeover time constant based on the recirculation rate, q_B, versus, the volume of fluid in the tank it is q_{tot}. All parameters except k_0, k_B, k_T, $\phi_{S,B}$, and $\phi_{S,T}$ are measured or estimable, other parameters might be estimated by independent experiments outside the scope of this study.

To test our model formulation we integrate equation 10 and divide any particular experiment's number density of crystals at steady-state (subscript i), with the result for a base case (subscript 1) to form a ratio, $R_{i,1}$—we assume that the supersaturation concentrations have not changed significantly, which is obviously an oversimplification. If we also assume that the ratio of crystal number densities will be approximated by the ratio of measured turbidity levels for those cases (NTU_i/NTU_1), then:

$$\frac{NTU_i}{NTU_1} = R_{i,1}^{\exp} \cong R_{i,1} \approx \frac{\tau_i}{\tau_1}\frac{\eta_{0,1}^2}{\eta_{0,i}^2}\frac{D_x + \frac{k_B}{k_0}\left[\frac{\eta_{0,i}^2}{\eta_{B,i}^2} q_{B,i} SV_B \phi_{S,B} + q_{tot,i} SV_T \phi_{S,T}\right]}{D_x + \frac{k_B}{k_0}\left[\frac{\eta_{0,1}^2}{\eta_{B,1}^2} q_{B,1} SV_B \phi_{S,B} + q_{tot,1} SV_T \phi_{S,T}\right]}. \tag{11}$$

Note, that since the surface area-to-volume ratios in the system, and the materials, are the same for all of our experiments, we used SV_B = 101.4 m^{-1} (= $SV_{B,1}$ = $SV_{B,i}$); SV_T = 41.1 m^{-1} (= $SV_{T,1}$ = $SV_{T,i}$); $\phi_{S,B} = \phi_{S,B,1} = \phi_{S,B,i}$; and $\phi_{S,T} = \phi_{S,T,1} = \phi_{S,T,i}$, in equation 11. We have also made the assumption that mixing and residence times don't change the values of the mass-action collision factors (*k*'s in equation 10), and that only the collision factors between the surface nucleation events and those in the bulk may be different, that is, all $k_{B,i}/k_{T,i} \sim 1$, and that material differences between surfaces can be resolved by varying the values of $\phi_{S,B}$ and $\phi_{S,T}$.

The key estimated parameters are the Kolmogorov mixing lengths for the bulk (and surface) in the CSTR tank, η_0, and for the recirculation tubing, η_B. The latter was initially estimated as described in section 2.2.2, by simple laminar flow pressure drop (f_D = 64/Re), but that approach failed to provide a reasonable correlation for the measured and forecasted ratios sought in equation 11. Since it is obvious that this peristaltic pumping flow would decidedly not be laminar flow[73-75], we applied an empirical modification for the friction factor during the peristaltic pumping in the recirculation tubing. We used a sigmoidal expression, whose contribution would decay as the *Re* increases,

$$f_{D,\mathrm{mod}} = f_D\left[1 + \frac{\mathrm{Re}}{a}\left(1 + \exp\left(k * (\mathrm{Re} - i)\right)\right)^{-1}\right] \tag{12}$$

where *k* controls the steepness of the response, *i* is the *Re* crossing at midpoint (0,1) and *a* is an arbitrary fitting magnitude. Values for these parameters were obtained during the regression analysis using the data in Table 7, such that

$$f_{D,\mathrm{mod}} \cong f_D\left[1 + \frac{\mathrm{Re}}{4}\left(1 + \exp\left(0.07 * (\mathrm{Re} - 437)\right)\right)^{-1}\right]. \tag{13}$$

Table 7 presents the experiments and measured turbidity levels used in our regression analysis for equation 11. The mixing length in the bulk (η_0) was estimated apriori and those for the recirculation tubing (η_B) resulted from regression on the parameters in equation 12 (shown in equation 13). Smaller mixing lengths means lower distances over which mass transfer must occur in order for species to "find each other" and nucleate and grow. The regression analysis also yielded the results that $k_B/k_0 = 1$; $\phi_{S,T} = 1$; and $\phi_{S,B} = 0.889$.

Table 7. Crystallization experiments (all τ ~3 min) with various levels of recirculation and impeller mixing and the associated mixing length scales used in modeling. The base case for our modeling was the 45 rpm impeller-only mixing experiment.

impeller speed (rpm)	recirculation rate (mL/min)	$^{1}\eta_0 \times 10^4$ (m)	$^{2}\eta_B \times 10^4$ (m)	turbidity (NTU)	type and level of mixing
45	380	2.1	1.05	64.0	impeller and recirculation
45	180	2.12	0.88	44.9	
45	90	2.12	0.77	30.9	
45	38	2.13	1.46	5.3	
45	19	2.13	2.44	1.8	
0	380	2.37	1.05	65.4	recirculation only
0	180	2.42	0.88	43.4	
0	90	2.42	0.77	27.9	
0	30	2.42	1.74	7.9	
0	20	2.42	2.35	3.6	
0	10	2.42	3.88	1.7	
45	0	2.13		2.2	impeller only
92	0	1.49		1.7	
132	0	1.17		2.2	

1 - mixing length scale in tank which includes (when applicable) impeller rotation, kinetic energy from continuous feed entry, and kinetic energy from recirculation flow entry.
2 - mixing length scale within the volume of the recirculation tubing.

Table 8. Definition of variables in the modeling.

variable	units	description
N_n	mol/m^3	no. of nuclei/vol (measured turbidity in NTU is an approximate determinate of this value)
dN_n/dt	mol/m^3/s	no. of nuclei/vol/time
C_c^*, C_a^*	mol/m^3	excess cation (Ca^{2+}) and excess anion (CO_3^{2-}) concentration versus saturation, respectively
D_x	m^2/s	ion pair diffusion coefficient $D_x \approx \dfrac{2}{\frac{1}{D_C}+\frac{1}{D_A}}$, 8.52×10^{-10}.
q_{tot}	m^3/s	total feed rate into the 1st CSTR
q_B	m^3/s	flowrate in the recirculation tubing

variable	units	description
SV_T, SV_B	m^{-1}	surface area to volume ratio of CSTR and recirculation tubing, respectively, e.g., $SV_T = S_{a,T}/V_0$.
η_B	m	Kolomogorov mixing length scale associated with the volume of fluid within the tubing during its period of movement within the tubing for recirculation
η_0	m	Kolomogorov mixing length scale associated with the volume of fluid within the tank
k_0, k_B, k_T	m^3/mol	mass-action collision factors due to efficiency of "collisions" culminating in a nucleation event in the bulk, in the recirculation tubing and CSTR, respectively.
$\phi_{S,T}$, $\phi_{S,B}$	-	fraction of the surface area with active sites favorable for nucleation events per unit area of the CSTR's surface and recirculation tube's surface, respectively (material property of crystal and material of the surface of CSTR/ tube). $0 \leq \phi_{S,T} \leq 1$, $0 \leq \phi_{S,B} \leq 1$
τ	s	CSTR residence time ($= V_0/q_{tot}$)
V_0, V_B	m^3	wetted volume of CSTR and recirculation tube, respectively
$S_{a,T}$, $S_{a,B}$	m^2	wetted surface area of CSTR and recirculation tubing, respectively

Figure 10 presents the correlation between the experimental turbidity ratios and the estimated nuclei concentration ratios (at steady-state) in a single CSTR after regression for the parameters in the modified friction factor relationship (equation 13). The correlation is weakest at the very low values of turbidity, where we also have the most uncertainty in our measurements. Also, it is pertinent to note that turbidity values in NTU units cannot be strictly correlated with crystal number density levels since size and shape of the crystals affect the NTU readings[61, 70, 76].

Nonetheless, the most heartening result from our modeling approach is that it points to promising ways to quantitatively combine the macroscopic variables relating to mixing efficiency and surface nucleation effects (heterogeneous nucleation) in the broad spectrum of crystallization reactors. In general, we found a similar relationship between energy dissipation (through the Kolmogorov length scale) and increased rate of nucleation crystal density as reported by Liu et al.[58] for the induction time (proportional to $\varepsilon^{-0.5}$ versus $\varepsilon^{-0.3}$ in the latter), and we identified an empirical method for including surface contacting time scales and chemistry. Interestingly, the regression analysis also suggested that the Norprene®—nominally a proprietary blend of polypropylene and poly(chloroprene)—in the recirculation tubing might be a less favorable surface for promoting $CaCO_3$ nucleation than the poly(methyl methacrylate), from which the CSTR tank is made. As yet, quantitative rules-of-thumb for the mechanisms underlying how surface chemistry influences crystallization (aka scaling) have not been developed, though several studies indicate interaction between the Ca^{2+} ion and the surface appears to be significant[77, 78]. In addition, water adsorption by the material also appears to increase mineral scaling[79]. Thus, our experimental and modeling methodologies may also be used to provide empirical metrics to differentiate material affects, including those from seed particles.

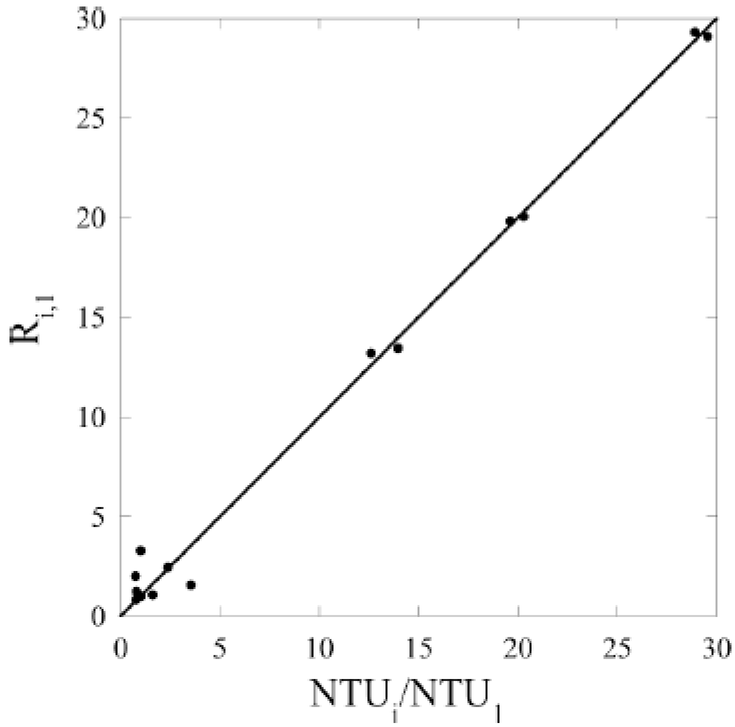

Figure 10. Correlation between predicted ratio of crystal number density and measured turbidity (NTU) using the case of 45 rpm without recirculation as the base case (as defined in equation 13). 45° line drawn to guide the eye.

3.4 Further discussion

Our methodology and results suggest that one cannot apriori state what the induction time or nucleation kinetics are for a specific crystallizer system without including some level of consideration for composition, both the mixing time and length scales, and heterogeneous nucleation. In addition, the latter appears to require a combination of surface area-to-volume ratio; contacting time scale, and the efficiency of the surface for enhancing crystallization for the particular precipitating species. Nonetheless, if a scaled up crystallizer system were to be dynamically and geometrically similar to the experiments presented in Figure 5 and Table 5, then one might estimate crystallizer sizing and costs based on ~66% supersaturation depletion after ~70 min of contact time, and use the slope of NTU vs time as an estimate of the kinetics. As a general comparison, other lab-scale studies of calcite crystallization with external enhancements, such as sonochemical[38] and seeds[80], indicate full supersaturation depletion within ~60 and 30 min, respectively. Whereas, Myasnikov et al.,[81] studied a broader range of variables and suggested that the duration of calcium carbonate crystallization varied from ~25 min for homogeneous crystallization, to ~3 min with the addition of $CaSiO_3$ seeds and ultrasound. Also, Tran et al.,[17] reported calcium removal on the order of 83% with a nominal reaction time of ~3 min in a ~2 m x 2 cm benchtop pellet softener system. Interestingly, large scale pilot tests (using pH adjustment) have operated solids contact reactors with residence times of 120 - 170 min[3, 15]. Thus, our nominal results appear more consistent with larger pilot tests than smaller bench-scale studies.

More importantly, our experimental approach facilitates systematic study of design changes for many specific crystallizer designs. As previously noted, pellet softening reactors are often piloted[13, 17, 82, 83] and, though it can only be approximated by CSTRs-in-series[62], our experimental protocol may be useful. For example, changes in pH and introduction of seed particles, which have often been evaluated, may be introduced at specific time points in the CSTRs to assess how/if an economic optimum may be reached for design and operation of pellet softener processes.

4 Conclusions

A reaction engineering approach to study crystallization of sparingly-soluble salts using CSTRs - in-series has been developed. Design scale-up factors using Kolmogorov mixing lengths, as well as, exposure times to surface area have been developed to quantify the apparent nucleation time (and crystallization rate), as indicated by turbidity measurements. It was found that mixing affects $CaCO_3$ crystal nucleation very significantly and is strongly dependent on the surface area-to-volume ratio of the mixing regions as opposed to simply power dissipation.

An improved and scalable metrology for obtaining nucleation and crystallization kinetics is needed to optimize the design of fluidized bed pellet softener reactors and other seeded (and unseeded) crystallizers. Currently, they are designed and piloted using very empirically-driven vs more mechanistically-inspired design heuristics. Thus, optimizing these systems is very difficult with so many variables, such as flow rate, seed/pellet content, variable feed concentrations, as well as, choosing proper seed material and addition of other materials, which might increase efficiency and make their outputs more predictable. In addition, industrial reports on pellet softening[84, 85], do not mention mixing effects or any design heuristics to account for them. Also, at least aspirationally, in desalination schemes, one would like to minimize the need for added mass agents (for example, base for pH titration and sacrificial seed materials). Thus, developing and studying an experimental protocol that is broadly applicable to the spectrum of crystallization mechanisms (homogeneous to heterogeneous) seems appropriate.

Further systematic study using our simple, empirical kinetic design model with more complex solutions, and varying geometrical and mass transfer parameters, is required to validate its possible general applicability for design of scaled-up crystallizers. Nonetheless, our experimental approach facilitates study of the nominal kinetic effects from perturbations in the process conditions and reaction environment around an initial steady-state. Such results can provide clearer directions for crystallization process improvements.

5 References

[1] M. Mickley, Membrane concentrate disposal: practices and regulation, in: Desalination and Water Purification Research and Development Program, Bureau of Reclamation, Denver, 2001.
[2] J. Glater, J.L. York, K.S. Campbell, Chapter 10 - Scale Formation and Prevention A2 - SPIEGLER, K.S, in: A.D.K. Laird (Ed.) Principles of Desalination (Second Edition), Academic Press, 1980, pp. 627-678.
[3] C.J. Gabelich, M.D. Williams, A. Rahardianto, J.C. Franklin, Y. Cohen, High-recovery reverse osmosis desalination using intermediate chemical demineralization, Journal of Membrane Science, 301 (2007) 131-141.
[4] M. Mickley, Brackish groundwater concentrate management, in: M. Associates (Ed.) State-of-Science White Paper, Boulder, CO, 2010.
[5] P. Xu, T.Y. Cath, A.P. Robertson, M. Reinhard, J.O. Leckie, J.E. Drewes, Critical review of desalination concentrate management, treatment and beneficial use, Environmental Engineering Science, 30 (2013) 502-514.
[6] B.K. Pramanik, L. Shu, V. Jegatheesan, A review of the management and treatment of brine solutions, Environ. Sci.-Wat. Res. Technol., 3 (2017) 625-658.
[7] A. Perez-Gonzalez, A.M. Urtiaga, R. Ibanez, I. Ortiz, State of the art and review on the treatment technologies of water reverse osmosis concentrates, Water Res., 46 (2012) 267-283.
[8] J. Leong, J. Tan, J. Charrois, B.P. Ladewig, Review of high recovery concentrate management options, Desalin. Water Treat., 52 (2014) 7609-7627.
[9] A. Subramani, J.G. Jacangelo, Treatment technologies for reverse osmosis concentrate volume minimization: A review, Sep. Purif. Technol., 122 (2014) 472-489.
[10] S.H. Joo, B. Tansel, Novel technologies for reverse osmosis concentrate treatment: A review, Journal of Environmental Management, 150 (2015) 322-335.
[11] J. Gilron, Chapter 12 - Brine Treatment and High Recovery Desalination A2 - Hankins, Nicholas P, in: R. Singh (Ed.) Emerging Membrane Technology for Sustainable Water Treatment, Elsevier, Boston, 2016, pp. 297-324.
[12] A. Giwa, V. Dufour, F. Al Marzooqi, M. Al Kaabi, S.W. Hasan, Brine management methods: Recent innovations and current status, Desalination, 407 (2017) 1-23.
[13] A.H. Mahvi, F. Shafiee, K. Naddafi, Feasibility study of crystallization process for water softening in a pellet reactor, International Journal of Environmental Science & Technology, 1 (2005) 301-304.
[14] A. Rahardianto, J.B. Gao, C.J. Gabelich, M.D. Williams, Y. Cohen, High recovery membrane desalting of low-salinity brackish water: Integration of accelerated precipitation softening with membrane RO, Journal of Membrane Science, 289 (2007) 123-137.
[15] C.J. Gabelich, A. Rahardianto, C.R. Northrup, T.I. Yun, Y. Cohen, Process evaluation of intermediate chemical demineralization for water recovery enhancement in production-scale brackish water desalting, Desalination, 272 (2011) 36-45.
[16] P. Sanciolo, E. Ostarcevic, P. Atherton, G. Leslie, T. Fane, Y. Cohen, M. Payne, S. Gray, Enhancement of reverse osmosis water recovery using interstage calcium precipitation, Desalination, 295 (2012) 43-52.
[17] A.T.K. Tran, Y. Zhang, N. Jullok, B. Meesschaert, L. Pinoy, B. Van der Bruggen, RO concentrate treatment by a hybrid system consisting of a pellet reactor and electrodialysis, Chem. Eng. Sci., 79 (2012) 228-238.

[18] S. Halevy, E. Korin, J. Gilron, Kinetics of gypsum precipitation for designing interstage crystallizers for concentrate in high recovery reverse osmosis, Industrial & Engineering Chemistry Research, 52 (2013) 14647-14657.
[19] E. Fountoukidis, Z.B. Maroulis, D. Marinoskouris, Modeling of calcium-sulfate fouling of reverse-usmosis membranes, Desalination, 72 (1989) 293-318.
[20] C.A.C. van de Lisdonk, J.A.M. van Paassen, J.C. Schippers, Monitoring scaling in nanofiltration and reverse osmosis membrane systems, Desalination, 132 (2000) 101-108.
[21] A.R. Greenberg, J. Gilron, K.D. Cobry, E. Kujundzic, X.Y. Lu, G. Mizrahi, M. Peterson, Analyzing ultrasonic signals using a dynamic window for an early detection of scaling in water processing equipment, in: USPTO (Ed.), Ben Gurion University of Negev Research and Development Authority Ltd and The Regents of the University of Colorado Boulder, USA, 2015.
[22] A.R. Bartman, E. Lyster, R. Rallo, P.D. Christofides, Y. Cohen, Mineral scale monitoring for reverse osmosis desalination via real-time membrane surface image analysis, Desalination, 273 (2011) 64-71.
[23] O. Sanni, O. Bukuaghangin, M. Huggan, N. Kapur, T. Charpentier, A. Neville, Development of a novel once-through flow visualization technique for kinetic study of bulk and surface scaling, Rev. Sci. Instrum., 88 (2017) 103903.
[24] P. Bots, L.G. Benning, J.-D. Rodriguez-Blanco, T. Roncal-Herrero, S. Shaw, Mechanistic insights into the crystallization of amorphous calcium carbonate (ACC), Crystal Growth & Design, 12 (2012) 3806-3814.
[25] R. Vacassy, J. Lemaitre, H. Hofmann, J. Gerlings, Calcium carbonate precipitation using new segmented flow tubular reactor, AlChE J., 46 (2000) 1241-1252.
[26] S.R. Dickinson, G. Henderson, K. McGrath, Controlling the kinetic versus thermodynamic crystallisation of calcium carbonate, J. Cryst. Growth, 244 (2002) 369-378.
[27] T. Chong, R. Sheikholeslami, Thermodynamics and kinetics for mixed calcium carbonate and calcium sulfate precipitation, Chem. Eng. Sci., 56 (2001) 5391-5400.
[28] S.R. Dickinson, K. McGrath, Switching between kinetic and thermodynamic control: calcium carbonate growth in the presence of a simple alcohol, J. Mater. Chem., 13 (2003) 928-933.
[29] K.J. Davis, P.M. Dove, J.J. De Yoreo, The role of Mg2+ as an impurity in calcite growth, Science, 290 (2000) 1134-1137.
[30] F. Manoli, E. Dalas, Spontaneous precipitation of calcium carbonate in the presence of ethanol, isopropanol and diethylene glycol, J. Cryst. Growth, 218 (2000) 359-364.
[31] B. Aziz, D. Gebauer, N. Hedin, Kinetic control of particle-mediated calcium carbonate crystallization, CrystEngComm, 13 (2011) 4641-4645.
[32] W. Al Nasser, A. Shaikh, C. Morriss, M. Hounslow, A. Salman, Determining kinetics of calcium carbonate precipitation by inline technique, Chem. Eng. Sci., 63 (2008) 1381-1389.
[33] D. Hasson, G. Sidorenko, R. Semiat, Calcium carbonate hardness removal by a novel electrochemical seeds system, Desalination, 263 (2010) 285-289.
[34] R. Sheikholeslami, M. Ng, Calcium sulfate precipitation in the presence of nondominant calcium carbonate: thermodynamics and kinetics, Industrial & engineering chemistry research, 40 (2001) 3570-3578.
[35] R. Sheikholeslami, H. Ong, Kinetics and thermodynamics of calcium carbonate and calcium sulfate at salinities up to 1.5 M, Desalination, 157 (2003) 217-234.

[36] W.M. Jung, S.H. Kang, W.-S. Kim, C.K. Choi, Particle morphology of calcium carbonate precipitated by gas–liquid reaction in a Couette–Taylor reactor, Chem. Eng. Sci., 55 (2000) 733-747.
[37] H.H. Teng, P.M. Dove, J.J. De Yoreo, Kinetics of calcite growth: surface processes and relationships to macroscopic rate laws, Geochim. Cosmochim. Acta, 64 (2000) 2255-2266.
[38] S. Shirsath, S. Sonawane, D. Saini, A. Pandit, Continuous precipitation of calcium carbonate using sonochemical reactor, Ultrason. Sonochem., 24 (2015) 132-139.
[39] M. Hong, H.H. Teng, Implications of solution chemistry effects: Direction-specific restraints on the step kinetics of calcite growth, Geochim. Cosmochim. Acta, 141 (2014) 228-239.
[40] D. Hasson, A. Cornel, Effect of residence time on the degree of CaCO 3 precipitation in the presence of an anti-scalant, Desalination, 401 (2017) 64-67.
[41] Q. Su, C.D. Rielly, K.A. Powell, Z.K. Nagy, Mathematical modelling and experimental validation of a novel periodic flow crystallization using MSMPR crystallizers, AlChE J., 63 (2017) 1313-1327.
[42] G. Cogoni, B. de Souza, P.J. Frawley, Particle size distribution and yield control in continuous plug flow crystallizers with recycle, Chem. Eng. Sci., 138 (2015) 592-599.
[43] S. Lawton, G. Steele, P. Shering, L. Zhao, I. Laird, X.-W. Ni, Continuous crystallization of pharmaceuticals using a continuous oscillatory baffled crystallizer, Organic Process Research & Development, 13 (2009) 1357-1363.
[44] A.J. Alvarez, A.S. Myerson, Continuous plug flow crystallization of pharmaceutical compounds, Crystal Growth & Design, 10 (2010) 2219-2228.
[45] R. Peña, J.A. Oliva, C.L. Burcham, D.J. Jarmer, Z.K. Nagy, Process intensification through continuous spherical crystallization using an oscillatory flow baffled crystallizer, Crystal Growth & Design, 17 (2017) 4776-4784.
[46] A.J. Alvarez, A. Singh, A.S. Myerson, Crystallization of cyclosporine in a multistage continuous MSMPR crystallizer, Crystal Growth & Design, 11 (2011) 4392-4400.
[47] M. Jiang, Z. Zhu, E. Jimenez, C.D. Papageorgiou, J. Waetzig, A. Hardy, M. Langston, R.D. Braatz, Continuous-flow tubular crystallization in slugs spontaneously induced by hydrodynamics, Crystal Growth & Design, 14 (2014) 851-860.
[48] S. Rosa, H.E.L. Madsen, Kinetics of mass crystallization of calcium carbonate at 25, 30 and 37 degrees C, J. Cryst. Growth, 318 (2011) 99-102.
[49] M.M. Reddy, G.H. Nancollas, The crystallization of calcium carbonate: I. Isotopic exchange and kinetics, J. Colloid Interface Sci., 36 (1971) 166-172.
[50] P. Agarwal, K.A. Berglund, In situ monitoring of calcium carbonate polymorphs during batch crystallization in the presence of polymeric additives using Raman spectroscopy, Crystal Growth & Design, 3 (2003) 941-946.
[51] H.N.S. Wiechers, P. Sturrock, G.V.R. Marais, Calcium-carbonate crystallization kinetics, Water Res., 9 (1975) 835-845.
[52] L.N. Plummer, E. Busenberg, The solubilities of calcite, aragonite and vaterite in CO2-H2O solutions between 0°C and 90°C, and an evaluation of the aqueous model for the system: CaCO3-CO2-H2O, Geochim. Cosmochim. Acta, 46 (1982) 1011-1040.
[53] W. Ostwald, Studien uber die Bildung und Umwandlung fester Korper, Z. Phys. Chem., 22U (1897) 289.
[54] J.C. Vanschouwenburg, Micro-EDTA titration of calcium: magnesium interference, Anal. Chem., 32 (1960) 709-711.

[55] E.M. Pouget, P.H.H. Bomans, J. Goos, P.M. Frederik, G. de With, N. Sommerdijk, The initial stages of template-controlled CaCO3 formation revealed by cryo-TEM, Science, 323 (2009) 1455-1458.
[56] R.S.K. Lam, J.M. Charnock, A. Lennie, F.C. Meldrum, Synthesis-dependant structural variations in amorphous calcium carbonate, Crystengcomm, 9 (2007) 1226-1236.
[57] D. Gebauer, A. Volkel, H. Colfen, Stable prenucleation calcium carbonate clusters, Science, 322 (2008) 1819-1822.
[58] J. Liu, M. Svard, A.C. Rasmuson, Influence of agitation on primary nucleation in stirred tank crystallizers, Crystal Growth & Design, 15 (2015) 4177-4184.
[59] L.D. Swinney, J.D. Stevens, R.W. Peters, Calcium carbonate crystallization kinetics, Industrial & Engineering Chemistry Fundamentals, 21 (1982) 31-36.
[60] G. Zhu, H. Li, S. Li, X. Hou, D. Xu, R. Lin, Q. Tang, Crystallization behavior and kinetics of calcium carbonate in highly alkaline and supersaturated system, J. Cryst. Growth, 428 (2015) 16-23.
[61] M. Parisi, A. Chianese, Investigation of nucleation kinetics by nephelometric measurements, Chemical Engineering & Technology, 36 (2013) 1335-1340.
[62] H.S. Fogler, Elements of Chemical Reaction Engineering, in: N.R. Amundson (Ed.) Prentice-Hall International Series in the Physical and Chemical Engineering Sciences, Prentice-Hall, Englewood Cliffs, NJ, 2006, pp. 1080.
[63] C. Pozrikidis, A study of peristaltic flow, J. Fluid Mech., 180 (1987) 515-527.
[64] E.L. Paul, V.A. Atiemo-Obeng, S.M. Kresta, Handbook of Industrial Mixing: Science and Practice, in, Wiley-Interscience, Hoboken, NJ, 2004.
[65] J. Saleh, The measurement of turbulence, in: Fluid Flow Handbook, McGraw-Hill Professional, New York, 2002.
[66] K.S. Raju, Piping, Seals, and Valves, in: Fluid Mechanics, Heat Transfer, and Mass Transfer: Chemical Engineering Practice, John Wiley & Sons, New York, 2011, pp. 768.
[67] A. Anderko, P. Wang, M. Rafal, Electrolyte solutions: from thermodynamic and transport property models to the simulation of industrial processes, Fluid Phase Equilib., 194-197 (2002) 123-142.
[68] H. Furukawa, Y. Kato, Y. Inoue, T. Kato, Y. Tada, S. Hashimoto, Correlation of power consumption for several kinds of mixing impellers, International Journal of Chemical Engineering, 2012 (2012) 6.
[69] W.Y. Shih, K. Albrecht, J. Glater, Y. Cohen, A dual-probe approach for evaluation of gypsum crystallization in response to antiscalant treatment, Desalination, 169 (2004) 213-221.
[70] H. Kleizen, A. De Putter, M. Van der Beek, S. Huynink, Particle concentration, size and turbidity, Filtration & separation, 32 (1995) 897-901.
[71] J.W. Mullin, K.D. Raven, Influence of mechanical agitation on the nucleation of some aqueous salt solutions, Nature, 195 (1962) 35.
[72] G. Capellades, S. Kiil, K. Dam-Johansen, M.J. Mealy, T.V. Christensen, A.S. Myerson, Effect of air injection on nucleation rates: an approach from induction time statistics, Crystal Growth & Design, 17 (2017) 3287-3294.
[73] J.C. Misra, S.K. Pandey, Peristaltic transport of a particle-fluid suspension in a cylindrical tube, Comput. Math. Appl., 28 (1994) 131-145.
[74] B.V.R. Kumar, K.B. Naidu, A numerical study of peristaltic flows, Comput. Fluids, 24 (1995) 161-176.

[75] S. Kumar, H.J. Kim, A. Beskok, Numerical simulations of peristaltic mixing, J. Fluids Eng.-Trans. ASME, 129 (2007) 1361-1371.
[76] M. Yao, J. Nan, T. Chen, Effect of particle size distribution on turbidity under various water quality levels during flocculation processes, Desalination, 354 (2014) 116-124.
[77] H. Deng, X.C. Shen, X.M. Wang, C. Du, Calcium carbonate crystallization controlled by functional groups: A mini-review, Front Mater Sci, 7 (2013) 62-68.
[78] E. Dalas, J. Kallitsis, P.G. Koutsoukos, The Growth of Sparingly-Soluble Salts on Polymeric Substrates, Colloids and Surfaces, 53 (1991) 197-208.
[79] Y.N. Wang, J. Davidson, L. Francis, Scaling in polymer tubes and interpretation for use in solar water heating systems, J Sol Energ-T Asme, 127 (2005) 3-14.
[80] P. Sanciolo, S. Gray, Effect of solution composition on seeded precipitation of calcium for high recovery RO of magnesium-bearing wastewater, surface water or groundwater, Sep. Purif. Technol., 172 (2017) 433-441.
[81] S.K. Myasnikov, A.P. Chipryakova, N.N. Kulov, Kinetics, energy characteristics, and intensification of crystallization processes in chemical precipitation of hardness ions, Theor. Found. Chem. Eng., 47 (2013) 505-523.
[82] W.D. Harms, R.B. Robinson, Softening by fluidized bed crystallizers, Journal of Environmental Engineering, 118 (1992) 513-529.
[83] C.W. Li, J.C. Jian, J.C. Liao, Integrating membrane filtration and a fluidized-bed pellet reactor for hardness removal, Journal - American Water Works Association, 96 (2004) 151-158.
[84] Innovative reclamation of membrane concentrates: conceptual evaluation of combining two innovative technologies in, Kennedy/Jenks Consultants, Irvine, California, USA (www.etcc-ca.com/sites/default/files/OLD/images/stories/pdf/ETCC_Report_321.pdf), 2005, pp. 45.
[85] N. Hantzsche, S. Itagaki, R. Ryder, September Ranch Subdivision Project Response to Comments to Draft REIR Appendix A: Water System Considerations -Background Technical Documents Appendix B: Condition Compliance and Mitigation Monitoring and Reporting Plan in, Kennedy/Jenks Consultants, Michael Brandman Associates, Questa Engineering Corporation., Monterey, CA, USA (www.co.monterey.ca.us/home/showdocument?id=37238), 2006.